Journal of Directed Energy, **3**, Fall 2008, 1–14

Effect of Natural Frequencies on Stresses in Impulsively Loaded Pressurized Thin-Walled Cylinders

George W. Sutton*

SPARTA, Inc., 1911 North Ft. Myer Drive, Suite 1100, Arlington, Virginia 22209

Robert Krech and William T. Laughlin

Physical Sciences, Inc., New England Business Center, Andover, Massachusetts 11810

Since the invention of lasers in 1960, there has been interest in their use for missile defense. Present interest is in their use for phase-boost intercepts that prevent the warhead from reaching its target while also preventing the deployment of penetration aids and/or submunitions. Whereas present programs are based on continuous-wave lasers, there is interest in powerful pulsed lasers that could burst a booster in a single pulse. Previous two-dimensional analyses have yielded large differences in results. To resolve this issue, vibration measurements were made on a pressurized steel tank. Experimentally measured vibration frequencies and pressure dependence agree with some of the previous researchers' results. Three-dimensional vibration modes were investigated theoretically and applied to a realistic solid-propellant-pressurized booster. Several megajoules of laser pulse energy are required to damage it, in agreement with those same previous researchers' results.

KEYWORDS: Booster, Composite, Damage, Laser, Pulsed

1. Introduction

There has arisen a large difference in the calculated impulse for a large single-laser pulse delivered to the side of a thin-walled pressurized cylindrical cylinder to cause the circumferential strain to exceed the yield strain. The induced strains are associated with the vibration modes, which depend on the vibration frequencies. In one analysis[9] a large impulse was required, but in subsequent analyses[5,6] a much lower impulse was found to be required. This paper reports on an experiment to determine the modal vibration frequencies and reexamines various theories of vibration; the experiment suggests a cause of the discrepancy that is quite interesting. The paper concludes with an estimate of the required laser pulse energy needed to damage a realistic solid-propellant booster while pressurized, using the current cylindrical shell analysis, in contrast to the previous analyses.

Received September 17, 2007; revision received February 11, 2008.
*Corresponding author; e-mail: George.Sutton@sparta.com.

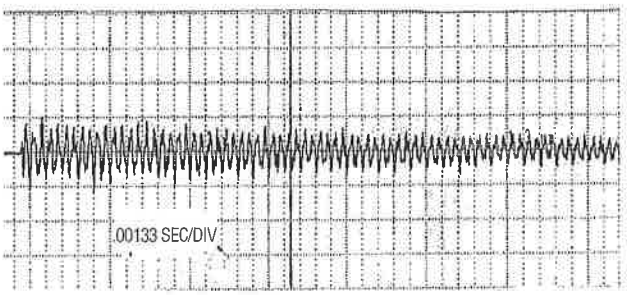

Fig. 1. Time history of strain gauge voltage measurements on opposite side of cylinder from impulse. Note the presence of harmonics by the nonsmoothness of the sinusoid. Time intervals: 0.0013 s.

Table 1. Mode frequencies of pressurized, thin-walled cylinder

	Frequency (Hz) at pressure (psig):	
Mode	0	1,000
First	1,495	1,630
Second	2,399	2,562

2. Experiment

A thin-walled steel cylinder ($h = 0.0009$ m, length $= 0.229$ m, and radius $= 0.0381$ m) had strain gauges attached to it at azimuthal angles θ of 30, 45, 90, and 135 deg. It was impulsed by a hammer at $\theta = 0$ deg, and the output of the strain gauges was recorded and the frequency analyzed. The vibrations generally damped out in 1/20 s. Two internal pressures were used, 0 and 100 psig. A typical record is shown in Fig. 1. Two main frequencies were observed, as shown in Table 1. The predictions of various theories are given in the Analysis section.

3. Analysis

An impulse load on the cylindrical side of a thin-walled circular cylinder induces various modes of vibration. The following three-dimensional (3D) vibrational displacement modes are used[2]:

$$\begin{aligned} u &= u_{mn} \cos(m\,\pi x/L) \cos n\theta \cos(\omega_{mn} t), \\ v &= v_{mn} \sin(m\,\pi x/L) \sin n\theta \cos(\omega_{mn} t), \\ w &= w_{mn} \sin(m\,\pi x/L) \cos n\theta \cos(\omega_{mn} t), \end{aligned} \tag{1}$$

where x is the axial direction from one end of the cylinder, y is in the radial direction at $\theta = 90$ deg, z is radially inward, L is the length of the cylinder, θ is the clockwise angle measured from the location of the impulsive loading, ω_{mn} is the angular frequency, and

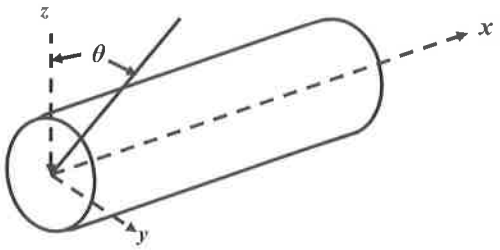

Fig. 2. Nomenclature for thin-walled shell.

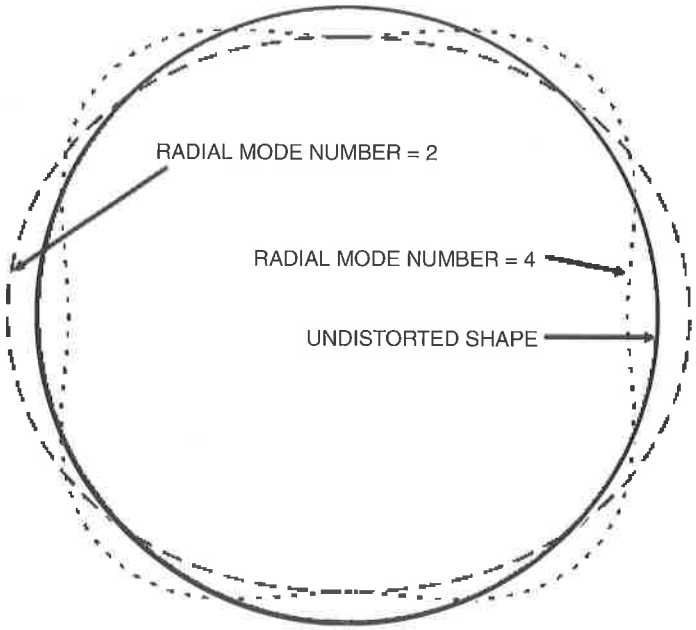

Fig. 3. Radial vibration modes of a cylinder.

u, v, and w are the displacements in the axial, tangential (clockwise), and radially inward directions. Figure 2 shows the nomenclature. These equations do not include any radial stresses in the shell that are caused by the impulse. If the impulse is delivered in a very short time, a radial compressive stress wave will be created, which when reflected from the inner wall of the shell could cause spallation. This has not been observed. But to be conservative, the impulse times considered here are longer than 100 μs, which is much shorter than any of the vibration response modes measured and calculated. Figure 3 shows the radial vibration modes.

From these modes, the strains can be calculated. The expressions for the relevant strains are[8]

$$\varepsilon_\theta = \frac{1}{r}\left(-w + \frac{\partial v}{\partial \theta}\right) + \frac{1}{2r^2}\left[\left(-w + \frac{\partial v}{\partial \theta}\right)^2 + \left(-\frac{\partial w}{\partial \theta} - v\right)^2 + \left(\frac{\partial u}{\partial \theta}\right)^2\right], \quad \text{(2a)}$$

Table 2. Frequencies calculated from the cubic equation

Pressure, psig	n, circumferential modal number	1st frequency, Hz	2nd frequency, Hz	3rd frequency, Hz
0	2	1,206	25,900	46,900
0	4	2,158	49,500	84,500
100	2	1,248	25,900	46,900
100	4	2,339	49,500	84,500

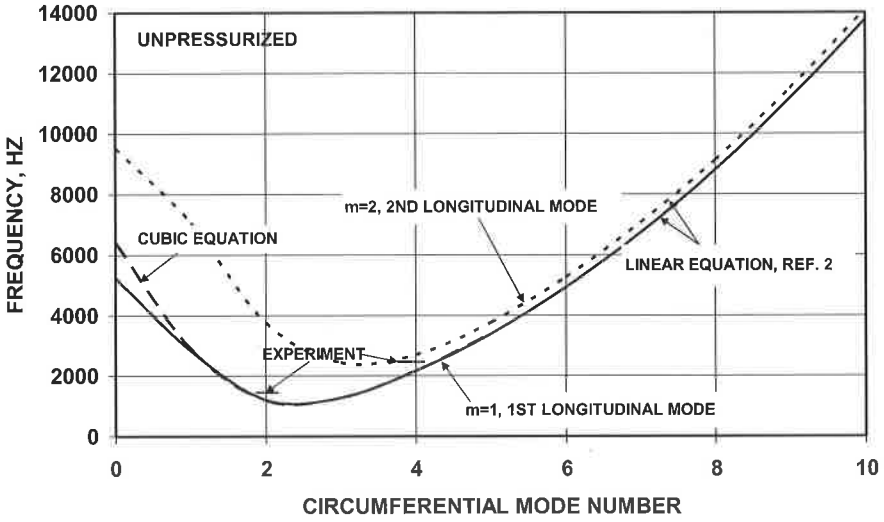

Fig. 4. Comparison of experimentally measured frequencies with shell theory for the unpressurized cylindrical steel tank.

$$\varepsilon_x = \frac{\partial u}{\partial x} + \frac{1}{2}\left[\left(\frac{\partial u}{\partial x}\right)^2 + \left(\frac{\partial v}{\partial x}\right)^2 + \left(\frac{\partial w}{\partial x}\right)^2\right], \tag{2b}$$

where r is the cylinder coordinate with mean radius of the cylinder $= a$. The Appendix contains the equations for the dynamic motion.[2]

To determine the strains, the mode coefficients must be found from the three equations of motion in the x, r, and θ directions. The mode coefficients are found after the equations of motion are solved to give the frequencies. Because there are three equations, the equation for the square of the frequencies is a cubic,[2] but in Ref. 2, only the lowest of three frequencies were given. For this experiment, the cubic equation was used to calculate all three (real) frequencies. These are given in Table 2.

The second and third frequencies were essentially independent of the internal pressure. It is interesting to note that low frequencies were reported in Refs. 5, 6, and 9, whereas high frequencies are given in Refs. 3, 5, and 6. (The last did not include bending.) A comparison of the experimental frequencies with the theory of Ref. 2 is shown in Fig. 4 for the unpressurized case.

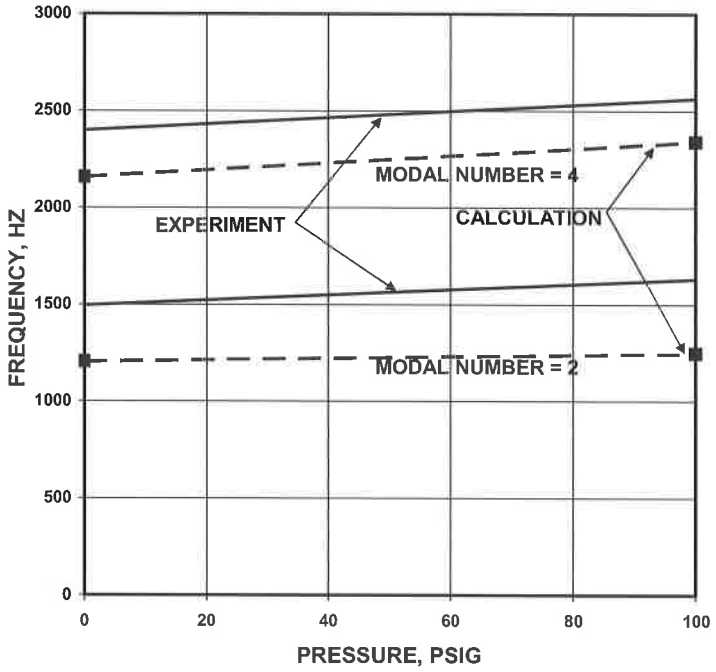

Fig. 5. Effect of internal pressurization on frequencies, 3D case.

It is seen that the theory of Ref. 2 agrees very well with the experimental lower frequencies for $m = 1$. The measured frequencies are slightly higher than the predicted frequencies. This may be caused by the end conditions: in Ref. 2, the ends of the cylinder are unconstrained, but in the experiment the ends of the cylinder are constrained by the end caps, which has the result of slightly increasing the frequencies.

The effect of pressurization of the cylinder is shown in Fig. 5. The calculations agree with the experiment in that the frequencies increase with pressurization. The lowest frequencies of Table 2 increase with pressure; the higher ones do not.

3.1. Infinitely long hollow cylinders of infinitesimal wall thickness, unpressurized

Next, a comparison is made of the vibration frequencies for infinitely long cylinders for which $m = 0$ with those predicted by Refs. 3, 5, 6, and 9 (Fig. 6). It is seen that both high and low frequencies are predicted in the various references. The highest frequencies were not detected. The meaning of the high frequencies can be discerned by examination of an infinitely long cylinder of infinitesimal wall thickness and zero pressure in which there is only v and w motion and circumferential bending is neglected. The equations of motion reduce to

$$\left(\frac{\omega_n^2}{\omega_o^2} - n^2\right) v_n + n w_n = 0,$$
$$n v_n + w_n \left(\frac{\omega_n^2}{\omega_0^2} - 1\right) = 0, \tag{3}$$

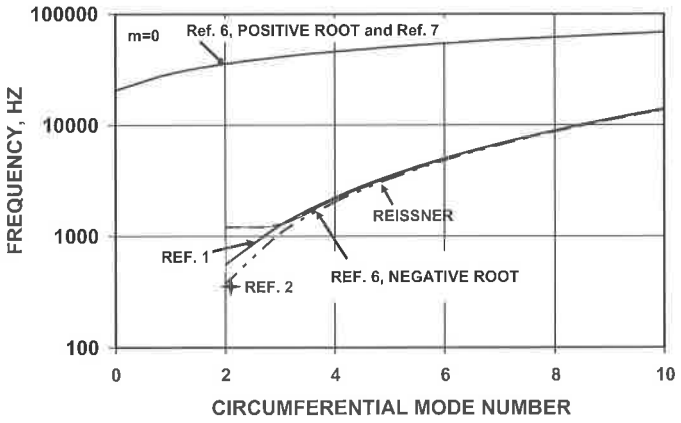

Fig. 6. Comparison of frequencies for an infinitely long cylinder ($m = 0$). Note the disagreements between various theories.

where $\omega_0^2 = E(1-v^2)/\rho a^2$, E is the elastic modulus, v is Poisson's ratio, and ρ is the density. The determinant of Eq. (3) must be zero, from which there are not one but two roots:

$$\frac{\omega_n^2}{\omega_o^2} = 0,$$
$$\frac{\omega_n^2}{\omega_o^2} = n^2 + 1. \tag{4}$$

The zero root was not mentioned previously.[3,4] For the zero root, the linear terms of the strain relation cancel out, leaving only the nonlinear terms, which gives a low strain for a given impulse. For this case a given impulse will lead to very low stresses. Hence the required impulse for damage is very high, as given in Ref. 9. The second root leads to high frequencies, for which the linear terms are additive. For this case a given impulse will lead to very high stresses. Hence there is a lower required impulse predicted in Refs. 5 and 6 to achieve excess strain. This is an interesting case, for when at $\theta = 0$ deg, w may be moving downward, at $\theta = 90$ deg, v is moving upward. It is difficult to understand how an impulse that drives the perimeter underneath it downward would drive the sides of the cylinder upward. In fact, Love[4] states that this mode "would be difficult to excite."

The smaller root is not zero when bending stresses are included but still remains small, compared to the two higher roots, as shown in Table 2. Note that for this root, when w moves radially downward, v is moving downward also. This is more satisfying physically than when v moves upward, as in the high-frequency case.

The issue of the circumferential vibrational mode was investigated experimentally by Rayleigh[7] on cylinders that were hollow at one end, a bell. He found that the lowest frequency corresponded to four nodal meridians, which means that $n = 2$. He did not state whether there were very high frequencies, of the order of (a/h); in other words, whether he observed the pure breathing mode. But the Fourier analysis plainly indicates that mode is excited. Nor did he comment on the $n = 1$ mode. Note that for the $n = 1$ mode, the two-dimensional frequency is zero and that when the portion of the shell at $\theta = 0$ (where the impulse is applied) moves in the direction of the impulse, so does the portion at $\theta = 90$ deg, which makes sense because the shell as a whole is moving downward due

to the impulse. If one accepts the lowest frequency (of the three) as most likely, then the second-order strain terms are also important. These were used in Ref. 9 and in part 3 of Ref. 2, except that the term $(-w+\partial v/\partial\theta)$ was omitted, which makes a 25% difference in the results.

3.2. Infinitely long hollow cylinders of finite wall thickness, pressurized

For this case, $u = m = 0$, and the equations of motion[2] reduce to

$$\begin{aligned}(b_2+\lambda)\,v_n + b_3 w_n &= 0,\\ c_2 v_n + (c_3+\lambda)\,w_n &= 0,\end{aligned} \tag{5}$$

where

$$\begin{aligned}b_2 &= -n^2\left(1+\frac{h^2}{12a^2}\right),\\ b_3 &= n\left(1+\frac{h^2}{12a^2}\right),\\ c_2 &= n\left[1+\frac{h^2}{12a^2}+\frac{a\left(1-\nu^2\right)p}{Eh}\right],\\ c_3 &= -1-n^4\frac{h^2}{12a^2}-n^2\frac{a\left(1-\nu^2\right)p}{Eh},\end{aligned} \tag{6}$$

where h is the cylinder wall thickness, p is the internal pressure of hollow cylinder, and

$$\lambda = \frac{a^2(1-\nu^2)\rho}{E}\omega_n^2.$$

The determinant of Eq. (5) is zero, which results in a quadratic equation for λ, the solution for which is

$$\lambda = \frac{-(b_2+c_3)\pm\sqrt{(b_2+c_3)^2-4(b_2c_3-b_3c_2)}}{2}. \tag{7}$$

This is irrational for h and $p > 0$. In accordance with the preceding discussion, the smallest root was chosen. This agreed very well with the results from solving the cubic equation[2] when $m = 0$. However, by taking advantage of the smallness of the terms with h and p, an expansion of Eq. (7) gives accurate results. It is given by

$$\omega_n^2 = \frac{n^2(n^2-1)E}{\rho a^2(1-\nu^2)}\left[\frac{(1-\nu^2)ap}{(n^2+1)Eh}+\frac{h^2}{12a^2}\right]. \tag{8}$$

Note that for $n = 0$, 1, the frequency is zero. This is also predicted from the cubic equation[2] when $m = 0$. With the frequencies determined, the ratio of v_n/w_n is found and the circumferential strains are calculated in accordance with Eq. (2).

4. Comparison with Explosive Impulse Tests

A comparison was also made to the SRI explosive impulse tests using the 3D theory. The parameters for the test were taken from Ref. 3. The tank was a composite, with a diameter

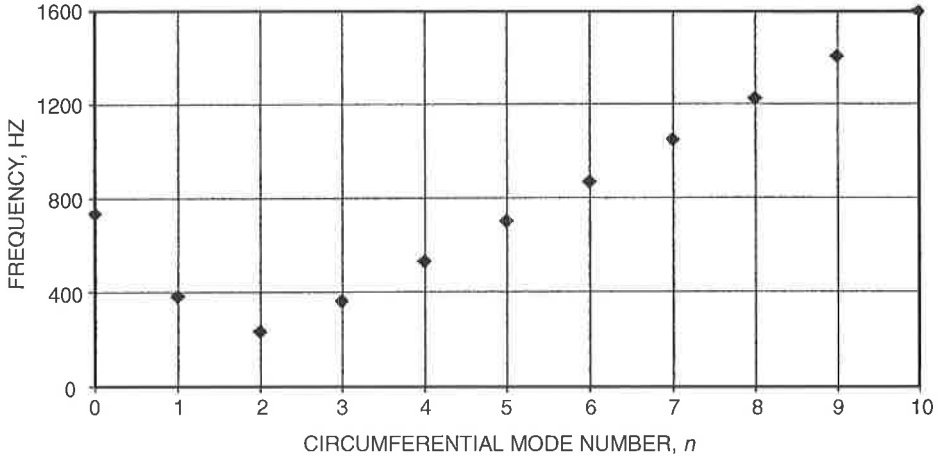

Fig. 7. Calculated distribution of lowest vibrational frequencies for the SRI test.

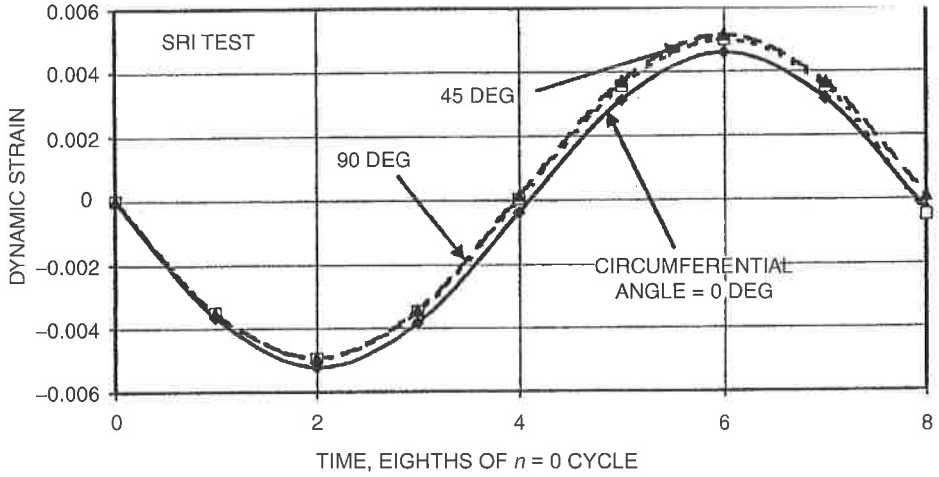

Fig. 8. Temporal circumferential strain history for SRI test.

of 50 cm and a 1-cm wall thickness, and had a layer of rubber on its interior to simulate the presence of a solid rocket propellant. Accounting for the mass of the simulated solid propellant (a factor of 6.7 × 1,200 kg/m^3), the resulting lowest mode frequency using the theory of Ref. 2 was 734 Hz, as compared to about ~731 Hz in the experiment.[1] No similar comparison was made in Ref. 3, 5, or 6. Composites generally fracture without plastic deformation.

Figure 7 shows the vibration frequencies for various circumferential modes for $m = 1$. The axial distribution of the impulse was not given in Ref. 3; herein it was approximated by $I_0 \sin(\pi x/L)$. Figure 8 shows the time history of the calculated dynamic circumferential strain for the total impulse of 123.5 N-s.

Because the dominant vibration mode is the breathing mode $n = 0$, there is not much variation in strain with circumferential angle θ. At 1/4 of the fundamental frequency cycle,

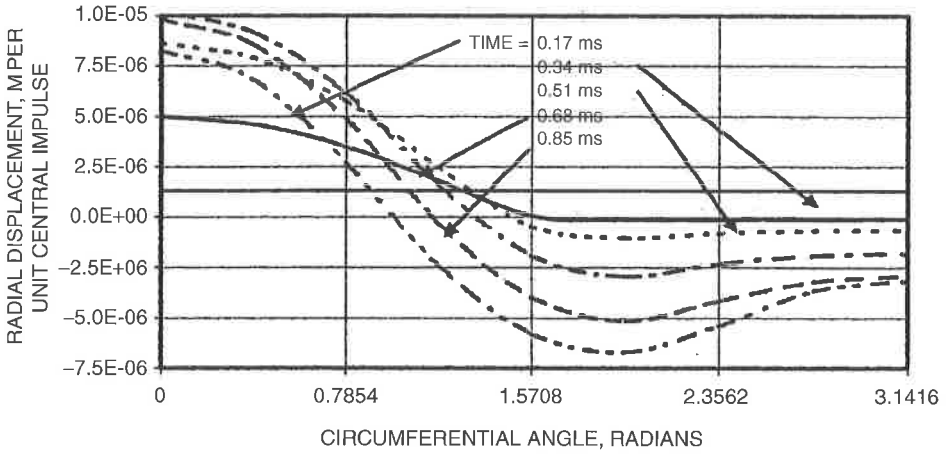

Fig. 9. Calculated radial motion history for the SRI test.

the total axial strain is calculated to be 1.36%, which did not cause failure. At 3/4 cycle, the calculated peak dynamic strain, 0.515%, agrees with the measured 0.50% dynamic strain for a total of 1.57% that resulted in failure.[1]

Assuming that there could be (an optimistic) pulse laser coupling coefficient of 10 dynes-s/J, a 1.52-MJ laser pulse would be needed to achieve this strain for the explosive impulse distribution used in the test. The maximum axial strain was calculated to be 1.65% at 45 deg and 1/4 cycle, but failure was not observed at this time in the test. If it had been assumed that the cylinder was infinitely long ($m = 0$), then for the breathing mode ($n = 0$) two frequencies are predicted by the cubic equation for frequency: 0 and 1,436 Hz, in agreement with Eqs. (4) but inconsistent with the measurements. The dynamic strain would have been 2.67%, which is much greater than the measurements. Thus, it is important that analyses be based on three dimensions for finite length cylinders, as presented herein.

The radial motion of the cylinder at the longitudinal center is shown in Fig. 9. Note that for short times, while the portion under the impulse is moving radially inward, the opposite side has not moved, which is in accordance with intuition.

5. Prediction for a Solid Propellant Rocket Motor Case

As an example of a realistic solid propellant upper-stage rocket booster, the Orbus 6 was chosen because its parameters are known, as shown in Table 3.

The shell wall density also accounts for the mass of unburned solid propellant, based on the results of Ref. 3. The 3D analysis was used. It is assumed that the laser wavelength is 0.25 μm, the beam quality is 1.4, the range is 4 Mm, and the beam director diameter is 4 m. The far field will then resemble a Gaussian of spatial standard deviation width of 0.1575 m. The pulse causes an impulse of the product of the fluence and the coupling coefficient C, optimistically assumed equal to 10 dynes-s/J. The impulse causes an initial radial inward motion given by

$$\rho h \dot{w}(\theta, t = 0) = I(\theta) \tag{9}$$

Table 3. Parameters of the Orbus 6 rocket motor

Parameter	Value
Material	Kevlar–epoxy
Diameter, m	0.804
Length, m	0.574
Elastic modulus, Pa	1×10^{11}
Internal pressure, Pa	4.16×10^{6}
Wall thickness, m	0.00889
Equivalent wall density, kg/m	1,329 × (1+7)

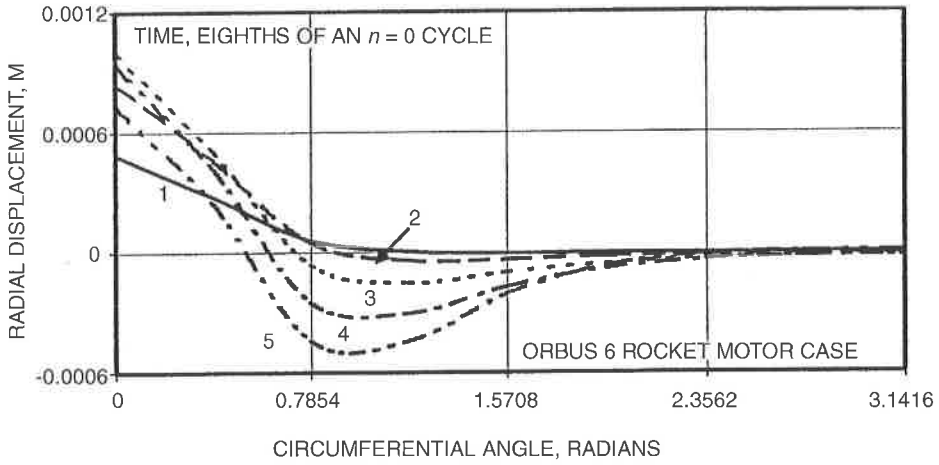

Fig. 10. Calculated radial displacements for an Orbus 6 pressurized rocket motor case.

or

$$\rho h \sum_{n=0,2,3,\ldots}^{\infty} \omega_n W_{nm} \sin(mx)\cos(n\theta) = I_0 \cos\theta * e^{-(x^2+y^2)/2\sigma^2}. \tag{10}$$

Fourier analysis was used to determine the values of W_{nm} and the equations of motion (5) to find U_{nm} and V_{nm} and Eq. (3) to find the strain. The value of the centerline impulse I_0 was chosen as a nominal 1,000 Pa-s.

The axial displacements are shown in Fig. 10. Note that at small times, only the portion exposed to the impulse moves, whereas later the entire case vibrates. The circumferential strains are shown in Fig. 11. They appear different from those of Fig. 8 because of the contribution, in this case, of $n > 0$ modes. The peak strain is 6.8×10^{-4} at 3/4 of the cycle time for $n = 0$.

The calculated axial strains are shown in Fig. 12. They reach a peak of 0.00186 earlier, at ~1/4 of the $n = 0$ cycle, and this is therefore the more stressing case. The static axial strain for this case is 0.0094. Assuming a safety margin of 50%, the maximum dynamic strain is 0.0047, a factor of 2.5 larger than that shown in Fig. 10. Thus, the peak impulse for failure should be about 2,500 Pa-s. The total impulse is $2\pi\sigma^2 I_0$ or 390 N-s. For an

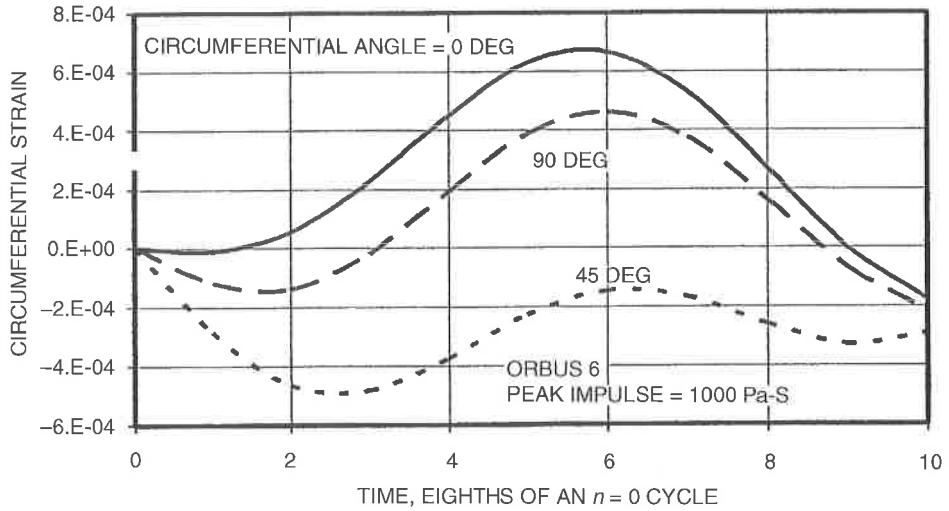

Fig. 11. Calculated circumferential strains for an Orbus 6 pressurized rocket motor case.

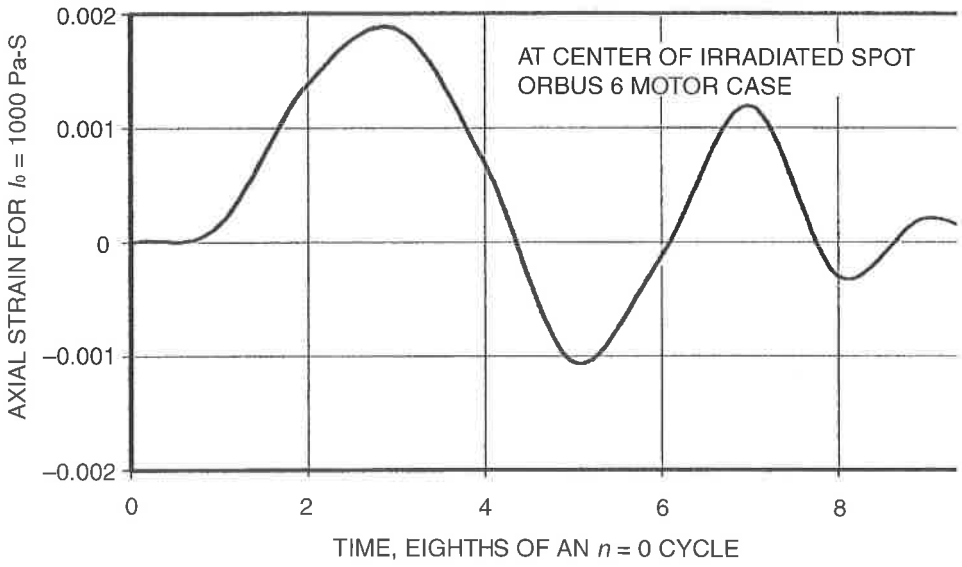

Fig. 12. Peak dynamic axial stress vs. time for the Orbus 6 rocket motor case.

optimistic laser impulse coupling coefficient of 10 dynes-s/J. this would require 3.9 MJ to exceed the maximum allowable strain.

6. Discussion

The above analysis extends previous analyses of an impulse on the side of a two-dimensional pressurized cylinder of infinite length to three dimensions for a pressurized cylinder of finite length. The cylindrical shell analysis results in three vibrational

frequencies, one low and two an order of magnitude higher. The vibrational frequencies directly influence the vibration modes and displacements in the various orthogonal directions, from which the strains are calculated. It is interesting that for the two-dimensional case there are two vibrational frequencies: one very high and one very low. Although the amplitude of vibration is inversely proportional to these frequencies, for the high-frequency mode the two linear terms for strain add so that the strain for a given impulse appears to be larger than for the low frequency. Also, the high-frequency mode has zero dependence on the internal pressure. For the low-frequency modes, the linear terms for strain largely cancel each other and the nonlinear terms dominate (except for $n = 0$). To resolve the differences, experiments were preformed on a pressurized steel cylinder. The vibrational frequencies were measured for various internal pressures. The frequencies and pressure dependence are in accordance with the lowest frequency 3D analysis. There have been no experimental observations of the two higher frequencies, but only of the lowest frequency, which was used herein. The comparison of the 3D analysis with the results of experiments on impulsively loaded pressurized cylinders showed good agreement.

The application of this 3D analysis to the case of a typical pressurized rocket motor, the Orbus 6, showed that for a Gaussian impulse distribution, corresponding to the far-field radiation distribution of a pulsed laser, a total impulse of 390 N-s would be needed to exceed its probable strain structural capability. If the laser impulse coupling coefficient is an optimistic 10 dynes-s/J, then a laser pulse energy of 3.9 MJ would be needed. This may be compared with the 1.8-MJ pulse at a cost of $3.89 billion delivered by the National Ignition Facility laser at Lawrence Livermore National Laboratory.

There are limitations to the 3D analysis presented above because the ends of the pressurized cylinder are free, whereas in the experiment and any application there are end bells on the cylinder. The next step to further clarify this should be a dynamic finite element structural analysis, which is beyond the scope of the current paper.

7. Appendix

$$\kappa^3 - K_2'\kappa^2 + K_1'\kappa - K_0' = 0$$

$$K_0' = K_0 + a_1\bar{n}_p + a_2\bar{n}_x + a_3\bar{n}_x\bar{n}_p + a_4\bar{n}_x^2 + a_5\bar{n}_p^2$$

$$K_1' = K_1 + b_1\bar{n}_p + b_2\bar{n}_x + [n^2\lambda^2/(1-\nu^2)^2] \times \bar{n}_x\bar{n}_\varphi + [\lambda^4/(1-\nu^2)^2]\bar{n}_x^2$$

$$K_2' = K_2 + [n^2/(1-\nu^2)]\bar{n}_\varphi + [2\lambda^2/(1-\nu^2)]\bar{n}_x$$

$$\kappa = (\rho a^2/E)\omega^2$$

$$\bar{n}_x = pa/2Eh$$

$$\bar{n}_\phi = pa/2Eh$$

$$\lambda = m\pi a/L$$

ν = Poisson ratio

n = circumferential mode number

$$(1-\nu^2)^3 K_0 = (1/2)(1-\nu)^2(1+\nu)\lambda^4 + (1/2)(1-\nu)(h^2/12a^2) \times [(\lambda^2+n^2)^4 - 2(4-\nu^2)\lambda^4 n^2 - 8\lambda^2 n^4 - 2n^6 + 4(1-\nu^2)\lambda^4 + 4\lambda^2 n^2 + n^4$$

$$
\begin{aligned}
(1-\nu^2)^3 K_1 &= (1/2)(1-\nu)(\lambda^2+n^2)^2 + (1/2)(3-\nu-2\nu^2)\lambda^2 + (1/2)(1-\nu)n^2 \\
&\quad + (h^2/12a^3)\times[(1/2)(3-\nu)(\lambda^2+n^2)^3 + 2(1-\nu)\lambda^4 - (2-\nu^2)\lambda^2 n^2 \\
&\quad - (1/2)(3+\nu)n^4 + 2(1-\nu)\lambda^2 + n^2] \\
(1-\nu^2)K_2 &= 1 + (1/2)(3-\nu)(\lambda^2+n^2) + (h^2/12a^2)[(\lambda^2+n^2)^2 + 2(1-\nu)\lambda^2 + n^2] \\
(1-\nu^2)^2 a_1 &= [(1-\nu)/2]n^2(n^2-\lambda^2)^2 - [(1-\nu)/2]n^4 + [\nu(1-\nu)/2]\lambda^4 \\
&\quad - [(2-3\nu-\nu^2)/2]\lambda^2 n^2 - \nu\lambda n - (h^2/12a^2)((\lambda^2+n^2)\{n^2\lambda^2 \\
&\quad + [(1-\nu)/2]n^4 + \nu\lambda n\} + [(1+\nu)/2]\lambda^2 n^2[(2-r)\lambda^2 + n^2 - (\lambda^2+n^2)^2]) \\
(1-\nu^2)^2 a_2 &= \lambda^2((1-\nu^2)\lambda^2 + [(1-\nu)/2][n^2 + (n^2-\lambda^2)^2] \\
&\quad + (h^2/12a^2)(\lambda^2+n^2)^2\{\lambda^2 + [(1-\nu)/2]n^2\}) \\
(1-\nu^2)^2 a_3 &= \lambda^2\{[(3-\nu)/2]\lambda^2 n^2 + [(1-\nu)/2]n^4 + \nu\lambda^2\} \\
(1-\nu^2)^2 a_4 &= \lambda^4\{\lambda^2 + [(1-\nu)/2]n^2\} \\
(1-\nu^2)^2 a_6 &= [(1+\nu)/2]\lambda^2 n^2(n^2-1) \\
(1-\nu^2)^2 b_1 &= [(3-\nu)/2]n^4 + 2\lambda^2 n^2 - n^2 + \nu\lambda^2 - (h^2/12a^2)n^2(\lambda^2+n^2) \\
(1-\nu^2)^2 b_2 &= [(5-\nu)/2]\lambda^4 + [(5-2\nu)/2]\lambda^2 n^2 + \lambda^2 + (h^2/12a^2)\lambda^2(\lambda^2+n^2)^2
\end{aligned}
$$

8. Acknowledgments

This work was partially supported by the Missile Defense Agency under contract HQOOO6-01-0058 Call 0003. This work was presented at the 35th Plasmadynamics and Lasers Conference, 28 June–1 July 2004, Portland, OR, as AIAA Paper 2204-2668.

References

[1]"Composite Bottle Thermomechanical Failure Analysis," ARA viewgraphs, courtesy of Stead Howie.

[2]Fung, Y.C., E.E. Sechler, and A. Kaplan, J. Aeronautical Sci. **54**(Sept.), 650 (1957).

[3]Lindberg, H.E., and Y.D. Murray, Aptek Report, February 24, 1988.

[4]Love, A.E.H., A Treatise on the Mathematical Theory of Elasticity, 4th ed., p. 454, Dover, New York (1927).

[5]Mirels, H., "Vibration of Pressurized Thin-Walled Cylinder Induced by Pulsed Laser—Addendum," Aerospace Report TOR-2001(1019)-1, August 2002.

[6]Mirels, H., and K. Zondervan, "Vibration of Pressurized Thin-Walled Cylinder Induced by Pulsed Laser," Aerospace Report TOR-2001(1019)-7, July 29, 2002.

[7]Rayleigh, Lord, Proc. Cambridge Phil. Mag. 5th Series, Sec. R., **VII**, 101 (1890).

[8]Saada, A.S., Elasticity, p. 138, Pergamon, New York (1974).

[9]Sutton, G.W. "High Energy Single Pulse Laser Structural Damage of Cylindrical Shells," 10th Annual AIAA/BMDO Technology Conference, July 23–26, 2001.

The Authors

Mr. Robert H. Krech, at Physical Sciences, Inc., has utilized shock and detonation waves to produce transient high-pressure and high-temperature conditions for the study of radiative energy transfer in hot gases and plasmas, low Earth orbit, and reentry environment simulations. He has studied laser and kinetic energy weapons, high-performance rocket propulsion concepts, chemical laser research, and sensor development. He has co-developed, patented, and manufactured high-flux atomic oxygen sources to study degradation of spacecraft materials in a low Earth orbit environment for NASA and the international aerospace community and developed an arc-driven shock tube facility to study the radiative

heat transfer during reentry. He was a member of an independent expert review panel for the NASA Ames EAST (Electrical Arc Shock Tube) Facility.

Dr. William T. Laughlin is responsible for program management of theoretical and experimental laser effects and laser lethality studies at Physical Sciences, Inc. He has performed numerous studies of laser effects on materials and the vulnerability of aerospace and ground targets to laser radiation. Experiments have been completed on a wide range of materials, using all laser wavelengths and waveforms. Target vulnerability analyses and tests have included IR and radar missiles, aircraft, UAVs, strategic missiles, and various ground targets, with studies on sensors, guidance electronics, engines, fuel tanks, warheads, flight control surfaces, solid rocket motors, and fuses. His work has included the development of optical instrumentation, target optical signatures measurement, and portable data acquisition devices. Dr. Laughlin pioneered the use of high-power lasers to simulate the severe thermal environments of rocket nozzles and high-speed flight for materials test and evaluation. He is a fellow of the Directed Energy Professional Society.

Dr. George W. Sutton developed the first atmospheric reentry heat shield used by long-range missiles and the first reconnaissance spacecraft. He pioneered aero-optics effects and several high-power lasers; was Editor-in-Chief of the *AIAA Journal* for 30 years; and is a member of the National Academy of Engineering. He has received numerous awards and authored more than 100 papers, 3 books, and several patents.